Available online at www.sciencedirect.com
ScienceDirect
Optics Communications 275 (2007) 94–103
OPTICS COMMUNICATIONS
www.elsevier.com/locate/optcom

Periodic pulse train conformation based on the temporal Radon–Wigner transform

Christian Cuadrado-Laborde [a,*], Pablo Costanzo-Caso [a], Ricardo Duchowicz [a], Enrique E. Sicre [b]

[a] Centro de Investigaciones Opticas (CIOp), Casilla de Correo 124, 1900 La Plata, Argentina
[b] Centro de Estudios Avanzados (CEAV), Universidad Argentina de la Empresa, Chile 1192, 1073 Buenos Aires, Argentina

Received 22 November 2006; received in revised form 8 March 2007; accepted 12 March 2007

Abstract

By using the Radon–Wigner transform (RWT), we analyze the temporal selfimaging or Talbot effect for producing well-conformed pulse trains with variable repetition rates and duty-cycles. The relationships linking the selfimaging conditions with the fractional orders of the RWT are first obtained for unchirped pulse trains. Then, we extend the analysis to chirped pulse sequences by deriving the conditions to be fulfilled by an equivalent unchirped pulse train producing the same selfimage irradiances. This result becomes relevant for observing well-defined high order fractional selfimaging, which are of interest due to their repetition rate multiplication. Besides, the effect of the finite extension of the pulse train on the selfimage quality is analyzed and a condition is found for relating the required minimum pulse number with the chirp parameter of the pulses.

Keywords: Pulse propagation; Temporal Talbot effect; Phase-space signal representations

1. Introduction

The development of techniques for the analysis and synthesis of ultrashort optical pulses has become of most importance in the field of optical communications, photonic signal processing and ultrafast optics. The characterization of the optical pulses can be performed from direct interferometric measurements in different domains such as time (t), frequency (v) or in a combined phase-space domain (t, v). Signal analysis using phase-space representations, like the Wigner distribution function (WDF), has been successfully applied to describe the system properties in several spatial optics applications [1–3]. Related with the WDF, a formalism based on the fractional Fourier transform (FRT) was developed in recent years to describe the properties of many optical devices in the spatial domain [4–10]. The FRT of a given optical signal can be also considered as a dual phase-space signal representation where the fractional order p varies from zero (only space information) to one (pure spatial frequency information). Several optical devices were proposed for implementing the spatial FRT, either through guided light transmission in a medium having a quadratic refractive index profile [4] or by combining lens action and free-space propagation [5]. Besides, an alternative interpretation of the FRT was given in connection with the Radon-Wigner transform (RWT) [7]. The RWT is obtained by performing a phase-space coordinate rotation of the WDF associated with the signal followed by a projection of this rotated WDF into the spatial frequency axis. An optical setup was proposed to implement the RWT of a one-dimensional input signal employing a varifocal lens device [9]. The RWT was successfully applied in signal processing as e.g., in the analysis and synthesis of multicomponent linear FM signals [11,12] and for enhancing resolution in ultrasound imaging [13].

* Corresponding author.
E-mail addresses: claborde@ciop.unlp.edu.ar (C. Cuadrado-Laborde), ricardod@ciop.unlp.edu.ar (R. Duchowicz), esicre@uade.edu.ar (E.E. Sicre).

0030-4018/$ - see front matter © 2007 Elsevier B.V. All rights reserved.
doi:10.1016/j.optcom.2007.03.021

On the other hand, the space–time duality theory was developed based on the analogy existing between the properties of quadratic-phase filters and Fresnel transforms in the spatial domain and the time impulse responses of different dispersive media and the frequency modulation of time-varying pulses in guided light transmission [14–18]. In this way, well known concepts and experiments developed in the framework of spatial optical systems can be transferred to the temporal domain thereby providing new ways for analyzing and processing time optical signals. Among several applications (as e.g., spectrum analyzers, temporal microscopy and pulse compression), temporal selfimaging or Talbot effect was implemented in order to produce periodic pulse trains with minimum distortion and different repetition rates [19–26]. Although selfimaging is a linear phenomenon, it has been also applied in connection with some nonlinear phenomena, such as Raman pulse compression [27], soliton generation [28] and cross-phase modulation [29].

In this paper we analyze the pulse trains conformation, which is produced from a proper combination of dispersive transmission and phase modulation applied to a periodic input signal, by employing an approach based on the temporal RWT and its connection with temporal selfimaging. To this end, we generalize a previously reported optical implementation of the RWT that is based on the space–time analogy and the theory of temporal imaging [30]. In that work, a relationship for obtaining the fractional orders p for which the FRT's coincide with a certain selfimaging condition was derived for the particular case of unchirped periodic pulse trains. Now, we extend the RWT signal description for analyzing pulse train conformation in the more realistic case of finite periodic pulse trains where the individual pulses are frequency chirped. The new conditions, for obtaining the fractional orders for which selfimages can be found, are derived by performing the analogy between our chirped pulse train and the equivalent unchirped pulse train, which would produce the same RWT at the specific fractional orders associated with selfimaging. The role of this unchirped pulse train is rather similar to the equivalent dispersion line which was used by Chantada et al. [31] in the spectral analysis of the temporal Talbot effect, without considering time lens action. We also investigate the relation between the number of pulses N that is required for obtaining a well-defined selfimage and the spectral content of the pulse trains. It is derived a relationship between N and the pulse chirp parameter which is corroborated in the numerical simulations.

In Section 2, we summarize the basic definitions of the FRT and the RWT in the spatial domain, together with the link between the FRT and the general spatial selfimaging. In Section 3, we introduce an optical definition of the RWT in the temporal domain. In Section 4, we analyze the temporal selfimaging by using the RWT formalism. The general relationships for producing integer and fractional selfimages of a finite, periodic chirped pulse train are obtained here. In Section 5, some numerical simulations are shown which illustrate the derived results. As we shall see, the previously found relationship between p and selfimaging, for the case of unchirped pulses, can be approximately applied for obtaining integer selfimages of an input chirped pulse train with small distortions. However, for the case of fractional selfimaging (which is of interest due to its repetition rate multiplication capability), the general relationships obtained here should be used for observing well-conformed pulse trains.

2. FRT and selfimaging: definitions and basic relationships in the spatial domain

The FRT can be defined explicitly in standard notation as an integral transform [4,5,10] as well as in several different ways [10]. We prefer to use the definition which involves a given rotation in the phase-space plane of the WDF [7,10]. The FRT of a given signal $u_0(x)$ can be found by performing the following steps

$$u_0(x) \rightarrow W_0(x,v) \rightarrow \widehat{R}_\phi[W_0(x,v)] \rightarrow |u_p(x)|^2 = \int_{-\infty}^{\infty} \widehat{R}_\phi[W_0(x,v)]\mathrm{d}v, \tag{1}$$

being

$$W_0(x,v) = \int_{-\infty}^{\infty} u_0\left(x+\frac{x'}{2}\right) u_0^*\left(x-\frac{x'}{2}\right) \exp(-2\pi i v x')\mathrm{d}x', \tag{2}$$

the WDF associated to the input signal, which is a dual signal representation defined in a phase-space: spatial coordinate (x) vs. spatial frequency (v). In Eq. (1), $\widehat{R}_\phi$ is the rotation operator acting on the WDF which changes $(x,v) \rightarrow (x',v') \equiv (x\cos\phi - v\sin\phi, v\cos\phi + x\sin\phi)$, being $\phi = p\pi/2$. Thus, the FRT modulus squared of $u_0(x)$ is obtained: (i) by passing to the WDF domain, (ii) rotating the WDF by an angle ϕ and (iii) by performing a projection into the spatial frequency axis. As these two last steps represent the Radon transform of a signal, $|u_p(x)|^2$ is also called the Radon–Wigner transform (RWT) of $u_0(x)$.

The FRT of a given one-dimensional space signal $u_0(x)$ can be optically implemented by properly combining lens action and light propagation. This combination can be performed either in a distributed or in a tandem way. In the first case, light transmission in a guided medium having a quadratic refractive index profile (like a GRIN medium) originate the successive FRT's of increasing fractional order p [4]. We focus our attention in the second approach where Lohmann proposed two simple setups for obtaining the FRT [5]. In one of them, the input signal $u_0(x)$ is illuminated by a monochromatic plane wave of wavelength λ, then interacts with a first lens of focal length f, then it propagates by a distance z, and it again interacts with a second lens having the same focal length f. The amplitude distribution after the second lens, which can be expressed as a proper scaled Fresnel integral, becomes the FRT of the input object being denoted as $u_p(x) \equiv \Im^{(p)}\{u_0(x)\}$ where $0 < p < 1$. The geometrical parameters are related with p as

$$z = f_0 \sin\left(\frac{p\pi}{2}\right), \tag{3a}$$

$$f = \frac{f_0}{\tan(p\pi/4)}, \tag{3b}$$

being f_0 a scaling factor. If $p = 0$ the FRT becomes $u_0(x)$, and if $p = 1$ the FRT becomes the normal Fourier transform of $u_0(x)$. For other values of p, the FRT exhibits both, mixed space and spatial frequency information about the input signal. As we are mainly interested in the light irradiance, $|u_p(x)|^2$ is the magnitude to be considered. As it was proved in [7], $|u_p(x)|^2$ displayed in a two-dimensional domain (x,p) becomes the RWT of the object $u_0(x)$. The RWT is a bilinear, phase-space signal description which is very useful in signal processing [11–13]. Thus, if a RWT display is obtained for $0 < p < 1$, the information about the input signal $u_0(x)$ continuously changes from a spatial representation ($p = 0$) to a pure spatial frequency description ($p = 1$).

The free-space diffraction originated by an input object under spherical illumination is closely related to the FRT production, as it was demonstrated in [9]. In the FRT setup described above, the first lens generates the spherical wave being the only difference with free-space diffraction the second lens action introducing a quadratic-phase factor. However, this effect is not relevant since the irradiance is the magnitude to be analyzed. Thus, if we choose the output plane placed immediately behind the second lens and we select the radius of the illuminating spherical wave $R = f$ and the propagation distance z accordingly with Eq. (3), the output irradiance $I_{\text{out}}(x)$ can be written as

$$I_{\text{out}}(x) = |\Im^{(p)}\{u_0(x)\}|^2 = |u_R(x;z)|^2, \tag{4}$$

where $u_R(x;z)$ is the Fresnel pattern diffracted by $u_0(x)$ a distance $z = f_0 \sin(p\pi/2)$ when the object is illuminated with a spherical wave of radius $R = f = f_0/\tan(p\pi/4)$. In the particular case of a periodic object $u_0(x) = t(x;d)$ (being d the spatial period), if $t(x;d)$, located at $z = 0$, is illuminated with a spherical wave converging to $z = R$, selfimages appear at the distances $z = sMd^2/\lambda$, being $M = (R - z)/R$ and $s = n/m$, where n and m are integers (see e.g., [21]). Two kind of selfimaging should be distinguished: (i) integer or Talbot selfimages, for which $s = n$ (i.e., $m = 1$), having periods $M \times d$, and (ii) fractional or sub-Talbot selfimages, for which n and m are coprime integers and $m \geqslant 2$, having periods $M \times d/m$. From these Talbot conditions, and by taking into account Eq. (4), the relationship between the selfimage patterns of $t(x;d)$ and the FRT is obtained as

$$|\Im^{(p)}\{t(x;d)\}|^2 = |t(x;d_T)|^2, \tag{5}$$

where the specific values $p = p_S$ for which Eq. (5) is satisfied are given by

$$p_S = \frac{2}{\pi}\tan^{-1}\left(\frac{sd^2}{\lambda f_0}\right), \tag{6}$$

and the selfimage period d_T results as

$$d_T = \frac{d}{m}\cos\left(\frac{p_S\pi}{2}\right). \tag{7}$$

Eqs. (5)–(7) include both fractional and integer selfimaging. The fractional orders associated with the integer selfimage conditions are derived from Eq. (6) by placing $m = 1$. Thus, for the fractional orders obtained from Eq. (6), the irradiance of the FRT (or equivalently, the RWT) becomes identical to demagnified replicas of the input periodic object with a period d_T given by Eq. (7). In the next section, we extend the RWT definition to the temporal domain for analyzing pulse train transmission in dispersive media using the space–time optical analogy. Pulse trains having a constant repetition rate are the equivalent time signals to the periodic objects of the spatial domain.

3. Temporal Radon–Wigner Transform (RWT)

The space–time duality theory is based on the mathematical analogy existing between the impulse response functions associated with spatial and temporal optical components. By using this analogy, pulse transmission devices can be developed having the same properties in the time domain that those having the amplitude distributions produced by the "analogue" or spatial counterparts [14–17]. In the temporal domain, a time lens introduces a quadratic-phase modulation into the time-varying signal. Besides, a dispersive medium (up to the first-order) has associated a quadratic-phase spectral response with a mathematical expression similar to that found in spatial Fresnel diffraction. In this way, through a suitable combination of dispersion and quadratic-phase modulation into the propagating pulses, time-domain analogues of a spatial imaging system can be synthesized. The equivalencies between spatial optics experiments and guided pulse propagation in dispersive media can be established in the following way

$$\lambda z \Longleftrightarrow 2\pi\Phi_{20}, \tag{8a}$$

$$\frac{2\pi}{\lambda f} \Longleftrightarrow \phi_{20}. \tag{8b}$$

In Eq. (8), z and f are the free-space propagation distance and the focal length, respectively, of the spatial optical system. Besides, Φ_{20} is the second-order dispersion coefficient of the medium where the pulses are transmitted (specified at the working central frequency $\omega = \omega_0$) and ϕ_{20} is the quadratic phase modulation factor associated with the time lens. The symbol $\Longleftrightarrow$ means that the magnitudes of the left side (spatial parameters) should be replaced by the magnitudes of the right side (time parameters) in order to produce the same impulse response (in case of spatial and time lenses) or the same transfer function (in case of Fresnel diffraction and dispersive pulse transmission).

The optical production of the spatial RWT was discussed in Section 2. By using Eq. (8), a photonic device for obtaining the temporal RWT associated with a time-varying signal $u_0(t)$ is shown in Fig. 1. The input light pulse first interacts

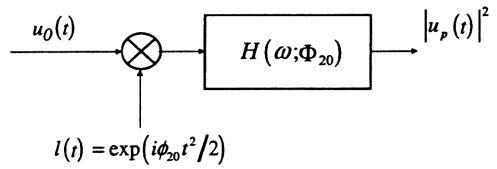

Fig. 1. Scheme of the optical device proposed to implement the temporal RWT. The input signal $u_0(t)$ is first phase modulated by $l(t)$ and then it is transmitted by the dispersive component having the transfer function $H(\omega) = \exp(i\Phi_{20}\omega^2/2)$. The output optical power is $|u_p(t)|^2$.

with a quadratic-phase modulator (having a phase modulation factor ϕ_{20}) and then with a dispersive medium having a second-order dispersion coefficient Φ_{20}, after which the resulting pulse is detected as $P_{\text{out}}(t) = |u_p(t)|^2$. It should be noted that as we are only interested in the signal irradiance (for producing the RWT), the second time lens that would be required for correcting the phase term of the FRT is not needed. Now, by applying Eqs. (3) and (8), the time-domain relationships linking the setup parameters Φ_{20} and ϕ_{20} with the fractional order p of $|u_p(t)|^2 = |\Im^{(p)}\{u_0(t)\}|^2$ result as

$$\Phi_{20} = \frac{\lambda\sigma_0}{2\pi}\sin\left(\frac{p\pi}{2}\right), \tag{9a}$$

$$\phi_{20} = \frac{2\pi}{\lambda\sigma_0}\tan\left(\frac{p\pi}{4}\right), \tag{9b}$$

where σ_0 is a scaling factor having dimensions of ps^2/nm rad. Thus, if the setup parameters Φ_{20} and ϕ_{20} are varied accordingly with Eq. (9), FRT modulus squared with a varying fractional order p are obtained from $P_{\text{out}}(t)$, i.e.,

$$P_{\text{out}}(t) = |\Im^{(p)}\{u_0(t)\}|^2 = \text{RWT}_{\phi=p\pi/2}\{u_0(t)\}, \quad 0 \leqslant p \leqslant 1, \tag{10}$$

Finally, two features should be kept in mind in the observation of the RWT displays of this work. First, since the set up parameters should be continuously changed to obtain $P_{\text{out}}(t) = |u_p(t)|^2$, for varying p, the temporal RWT of the input signal is sequentially produced. Second, there is a pulse delay effect that directly depends with p (through Φ_{20}, see Eq. (9a)) which, if it is not compensated, would originate a shear display of the RWT [30]. Therefore, to facilitate the comparison between different fractional orders p, all RWT displays of this work were temporally aligned with the input, and thus they do not show this shear effect.

If the complete temporal RWT is to be photonically realized, it should be taken into account that the setup parameters Φ_{20} and ϕ_{20} are continuously changed accordingly with Eq. (9) for obtaining $P_{\text{out}}(t) = |u_p(t)|^2$ for varying p. Therefore, the complete RWT display of the input signal can only be sequentially produced and it would require a dispersive medium with a well-controlled second-order coefficient and time lenses with different phase modulation factors. By this reason, we propose a numerical implementation of the RWT in order to achieve the whole display ($0 < p < 1$) for signal analysis purposes and, when a particular value $p = p_0$ is selected depending on the pulse transmission required application, the optical device is only once implemented with the parameters Φ_{20} and ϕ_{20} obtained from Eq. (9) by replacing $p = p_0$.

4. Periodic pulse train conformation with different repetition rates

A very important application related with the spatial-temporal analogy is the temporal selfimaging or Talbot effect where conformation of periodic pulse trains having different repetition rates can be achieved by properly combining signal phase modulation (or time lens action) with pulse transmission in guided dispersive media [19–29]. Although this subject was extensively treated by many authors, there are several features that can be conveniently analyzed employing the RWT approach.

By using the photonic device sketched in Fig. 1, and by considering as input signal $u_0(t)$ a sequence of N pulses having a pulse width T_0 and a repetition period T_1, the output optical power becomes $P_{\text{out}}(t) = |\Im^{(p)}\{u_0(t)\}|^2$, whenever the setup parameters Φ_{20} and ϕ_{20} are related with p in accordance with Eq. (9). Besides, by taking into account Eqs. (5)–(7) linking the selfimage patterns and the FRT of a periodic spatial object, a temporal analogue condition can be found as

$$P_{\text{out}}(t) = |\Im^{(p)}\{u_0(t)\}|^2 = |u_0(t/M)|^2, \tag{11}$$

where the selfimage magnification factor M is given by

$$M = \frac{\cos(p_S\pi/2)}{m}. \tag{12}$$

The specific values $p = p_S$ for which the FRT becomes a temporal selfimage, as given by Eq. (11), can be found by transforming Eq. (6) to the time domain, so resulting

$$sT_1^2 = \lambda\sigma_0\tan\left(\frac{p_S\pi}{2}\right), \tag{13}$$

where, as in the spatial case, $s = n$, with $n = 1, 2, 3, \ldots$, for the integer or Talbot selfimages and $s = n/m$ (being n and m coprime integers and $m \geqslant 2$) for the fractional or sub-Talbot selfimages. The main difference between integer and fractional selfimaging, as replicas of the input pulse train, are: (i) the repetition rates are $T_1 x \cos(p_S\pi/2)$ and $T_1/mx\cos(p_S\pi/2)$ for integer and fractional selfimages, respectively, and (ii) the duty-cycle T_0/T_1 remains unchanged for the integer selfimages while it is multiplied by m for the fractional selfimages. In this way, if the whole RWT display is generated from a given input pulse train $u_0(t)$, output pulse trains having different repetition rates, and equal or different duty-cycles, can be produced by choosing the setup parameters Φ_{20} and ϕ_{20} in accordance with the selected values of p_S.

For establishing the spatial–temporal selfimaging analogy, periodicity becomes an essential condition. In the spatial domain, a finite object may easily have $N \cong 10^3$

diffracting lines, being its space-bandwidth product large enough for considering it as a periodic object. In this case, a large number of well-defined selfimages can be observed. The situation is completely different in the temporal domain. Although pulse trains having constant repetition rate and time duration long enough as to be considered a periodic time signal can be implemented, the actual number N of consecutive pulses which can be phase-modulated by a practical time lens and/or spectral overlapped by the employed dispersive medium is rather limited. By this reason, it is very important to establish the minimum number of pulses $N = N_0$ in order to obtain well-formed temporal selfimages. This question was first analyzed by Azaña [26]. By considering the total time-bandwidth product K_{env} associated with the envelope of the pulse train, the selfimaging conditions and the relation $N \approx \Delta t_{\text{env}}/T_1$, being Δt_{env} the total temporal duration of the pulse train, they derive the following inequality

$$N_0 \gg \frac{K_{\text{env}} s T_1}{2\pi T_0}, \tag{14}$$

where $s = n/m$ characterizes the selfimage. Basically, this relation states that N_0 should be large enough as compared with the reciprocal of the pulse train duty-cycle. We here analyze this question choosing as periodic input signal $u_0(t)$ a pulse train of N Gaussian-profile pulses, with repetition rate T_1, which can be expressed as

$$\begin{aligned} u_0(t) &= A_0 \sum_{k=-N/2}^{N/2} \exp\left[-\frac{(1+\mathrm{i}C)}{2T_0^2}(t-kT_1)^2\right] \\ &= \operatorname{rect}\left(\frac{t}{NT_1}\right) \times \sum_{q=-\infty}^{\infty} a_q \exp(\mathrm{i}2\pi q t/T_1), \end{aligned} \tag{15}$$

where A_0 is the pulse maximum amplitude, T_0 is the half-width (measured at $1/e$ decay in power), C is the chirp parameter and $\operatorname{rect}(t/\Delta t) = 1$ in a time interval $\Delta t \cong NT_1$. The Fourier coefficients a_q become

$$a_q \cong a_0 \exp\left[-\frac{2\pi^2 T_0^2}{(1+\mathrm{i}C)T_1^2} q^2\right]. \tag{16}$$

In the spatial selfimaging, the so-called "walk-off" effect or lack of in-phase interference due to the spatial separation of the several diffracted orders, determines the maximum number of observable selfimages. Basically, the maximum selfimage distance z_T is limited by the relationship $\tan\alpha_c = Nd/z_T \cong q_c\lambda/d$, being Nd the spatial extent of the finite periodic object, q_c the maximum diffracted order that is present in the selfimage and α_c the angle subtended with the optical axis which satisfies the grating condition $d\sin\alpha_c = q_c\lambda$. By translating this result to the temporal domain, by using Eqs. (8a) and (9a), we obtain

$$N_0 \cong \frac{q_c \lambda \sigma_0}{T_1^2} \sin(\pi p_S). \tag{17}$$

As $|a_q|^2$ is the optical power of the q-diffracted order, we limit the infinite Fourier expansion of Eq. (15) to a finite Fourier series up to a maximum order q_c such as $|a_{q_c}/a_0|^2 \cong 0.1$, i.e., we neglect all the orders $q > q_c$ having optical powers lower than 10% of that associated with the zero-order. This criterion yields to different results depending on the shape of the individual pulses but it becomes adequate for slow-varying functions like Gaussians. Thus, q_c can be derived, by using Eq. (16), from the condition

$$\left|\frac{a_{q_c}}{a_0}\right|^2 \cong \exp\left[-\frac{4\pi^2 T_0^2}{(1+C^2)T_1^2} q_c^2\right] \cong 0.1. \tag{18}$$

For a duty-cycle $T_0/T_1 = 0.05$, it can be obtained $q_c = 5$ for $C = 0$ and $q_c = 30$ for $C = -6$. This means that the pulse number N of the chirped pulse train should be increased by a factor $|C|$ as compared with the unchirped pulse train for obtaining the same selfimage quality. This fact will be further illustrated in the next section where some examples were presented. Now, we are interested in deeper analyze the selfimage formation when pulse chirping is present by taking advantage of the RWT formalism. As the procedure for obtaining the RWT, as shown in Fig. 1, consists of a quadratic-phase modulation of the input signal $u_0(t; C)$ by a time lens $l(t)$ followed by dispersive propagation (which is mathematically equivalent to delay the signal spectrum by a quadratic transference function $H(\omega)$), we can express the output amplitude as

$$\begin{aligned} u_{\text{out}}(t) &= [u_0(t)l(t)] \otimes h(t) \\ &= [u_0(t)\exp(\mathrm{i}\phi_{20}t^2/2)] \otimes \exp(-\mathrm{i}t^2/2\Phi_{20}), \end{aligned} \tag{19}$$

being $h(t) = \Im^{-1}\{H(\omega)\}$ the impulse response associated with the dispersive component and $\otimes$ denotes convolution. By calculating Eq. (19), it can be written as

$$\begin{aligned} u_{\text{out}}(t) \cong K &\exp\left[-\mathrm{i}\left(1-\frac{1}{1-\Phi_{20}\phi_{20}}\right)\frac{t^2}{2\Phi_{20}}\right] \\ &\times \sum_{q=-\infty}^{\infty} \exp\left[-\frac{2\pi^2 T_0^2}{(1+C^2)T_1^2} q^2\right] \\ &\times \exp\left[\mathrm{i}\frac{2\pi^2}{T_1^2}\left(\frac{CT_0^2}{1+C^2}+\frac{\Phi_{20}}{1-\phi_{20}\Phi_{20}}\right)q^2\right] \\ &\times \exp\left[\mathrm{i}\frac{2\pi q t}{(1-\phi_{20}\Phi_{20})T_1}\right], \end{aligned} \tag{20}$$

where K is a complex constant and the approximation $\Delta t \cong NT_1 \gg T_0$ was used. Thus, the RWT associated with the chirped pulse train can be obtained from Eq. (20) as

$$P_{\text{out}}(t) = |\Im^{(p)}\{u_0(t; C)\}|^2 \cong \left|K \sum_{q=-\infty}^{\infty} b_q \exp\left[\mathrm{i}\frac{2\pi q t}{MT_1}\right]\right|^2, \tag{21}$$

being

$$\begin{aligned} b_q = &\exp\left[-\frac{2\pi^2 T_0^2}{(1+C^2)T_1^2} q^2\right] \\ &\times \exp\left[\mathrm{i}\frac{2\pi^2}{T_1^2}\left(\frac{CT_0^2}{1+C^2}+\frac{\Phi_{20}}{1-\phi_{20}\Phi_{20}}\right)q^2\right], \end{aligned} \tag{22a}$$

$$M = 1 - \phi_{20}\Phi_{20}, \tag{22b}$$

and the parameters Φ_{20} and ϕ_{20} are varied accordingly with Eq. (9) for obtaining the whole RWT display for $0 < p < 1$.

Let us now investigate the relationship between the RWT, as given by Eq. (21), and the selfimaging formation. For the particular case of an unchirped pulse train, this relationship was previously given by Eqs. (11)–(13). Thus, we reformulate the problem in the following way. We analyze the properties of the unchirped pulse train $\hat{u}_0(t; C = 0)$ that would produce the same RWT for selfimaging as it is given by the output irradiance of Eq. (21). If $\widehat{T}_1$ and $\widehat{T}_0$ denote the repetition rate and pulse width of $\hat{u}_0(t; C = 0)$, then the output irradiance can be obtained by properly using Eqs. (21) and (22) with $C = 0$, i.e.,

$$P_{\text{out}}(t) = |\Im^{(p)}\{\hat{u}_0(t; C = 0)\}|^2 \cong \left| K \sum_{q=-\infty}^{\infty} \hat{b}_q \exp\left[i \frac{2\pi q t}{\widehat{M}\widehat{T}_1} \right] \right|^2, \tag{23}$$

where $\hat{b}_q$ and $\widehat{M}$ are now given as

$$\hat{b}_q = \exp\left[-\frac{2\pi^2 \widehat{T}_0^2}{\widehat{T}_1^2} q^2 \right] \exp\left[i \frac{2\pi^2 \widehat{\Phi}_{20}}{\widehat{M}\widehat{T}_1^2} q^2 \right], \tag{24a}$$

$$\widehat{M} = 1 - \hat{\phi}_{20}\widehat{\Phi}_{20}, \tag{24b}$$

where the unknown values of $\widehat{\Phi}_{20}$, $\hat{\phi}_{20}$, $\widehat{T}_1$ and $\widehat{T}_0$ are to be determined by equalizing Eqs. (23) and (21), since the same output irradiance was required. From this condition, we derive the following three relationships

$$MT_1 = \widehat{M}\widehat{T}_1, \tag{25a}$$

$$\frac{1}{1 + C^2}\left(\frac{T_0^2}{T_1^2}\right) = \frac{\widehat{T}_0^2}{\widehat{T}_1^2}, \tag{25b}$$

$$\frac{C}{1 + C^2}\left(\frac{T_0^2}{2T_1^2}\right) + \frac{\Phi_{20}}{2MT_1^2} = \frac{\widehat{\Phi}_{20}}{2\widehat{M}\widehat{T}_1^2}. \tag{25c}$$

By using Eq. (25), we intend to solve the following question. We have two different pulse trains: (i) one chirped $u_0(t; C)$ having known parameters $(T_1, T_0, C \neq 0)$ for which the fractional orders p_S associated to the selfimages are unknown; (ii) a second unchirped pulse train $\hat{u}_0(t; C = 0)$, with $\widehat{T}_1$ and $\widehat{T}_0$ as unknown parameters, for which the fractional order $\hat{p}_S$ corresponding to a selfimage condition can be obtained from Eq. (13) (since $C = 0$), i.e.,

$$\hat{p}_S = \frac{2}{\pi} \tan^{-1}\left(\frac{s\widehat{T}_1^2}{\sigma_0 \lambda} \right), \tag{26}$$

Unfortunately, Eq. (26) can not be solved since $\widehat{T}_1$ is unknown. However, by returning to the previous heuristic analysis (Eqs. (15)–(18)), we conclude that the main difference between chirped and unchirped pulse trains for producing selfimaging lies in the number of required Fourier coefficients rather than periodicity. Hence, we introduce the condition $\widehat{T}_1 \cong T_1$, approximation which is to be justified from the results shown in the next section. Now, we can solve Eq. (26) for obtaining $\hat{p}_S$. By using Eqs. (25a) and (25c), together with Eq. (9), we derive the following relationship to found the values of p_S

$$\tan\left(p_S \frac{\pi}{2}\right) = \tan\left(\hat{p}_S \frac{\pi}{2}\right) - \frac{C}{1 + C^2}\left(\frac{2\pi T_0^2}{\sigma_0 \lambda}\right). \tag{27}$$

Finally, from Eq. (25b) it results

$$\frac{T_0^2}{1 + C^2} = \widehat{T}_0^2. \tag{28}$$

Thus, we arrive to the following result: The selfimages produced by a chirped Gaussian pulse train $u_0(t; C)$, with pulse width T_0 and repetition rate T_1, which are observed at $p = p_S$ in its RWT display, are the same selfimages originated by an unchirped Gaussian pulse train $\hat{u}_0(t; C = 0)$, having the same repetition rate $\widehat{T}_1 = T_1$ and pulse width $\widehat{T}_0 = T_0/\sqrt{1 + C^2}$, obtained at $p = \hat{p}_S$ (derived from Eq. (26) with $\widehat{T}_1 = T_1$) in its corresponding RWT display. The relationship linking p_S and $\hat{p}_S$ is given by Eq. (27) being their main difference the term involving $CT_0^2/\sigma_0\lambda(1 + C^2)$. As we shall see in the next section, for the first selfimage ($s = 1$) and its associated fractional selfimages ($s = 1/m$, with $m \geqslant 2$), with $C = -6$, $\sigma_0 = 1.42$ ps^2/nm rad and $\lambda = 1550$ nm, from Eq. (27) it can be obtained $p \cong 1.001\hat{p}_S$. However, this slight variation in the selected fractional order of the RWT becomes very important for observing or not fractional selfimaging of high repetition rate multiplication ($m > 10$). As a final remark, Chantada et al. recently presented a spectral analysis of the temporal Talbot effect by only employing fiber dispersive lines [31]. The relationships we obtained between Φ_{20} and $\widehat{\Phi}_{20}$ (as given by Eq. (25c)) (or equivalently, between p_S and $\hat{p}_S$ as given by Eq. (27)) using the tandem time lens-dispersive line of Fig. 1, reduce to the equivalent dispersion defined in Eq. (5) of [31], when unitary magnification $M = \widehat{M} = 1$ is considered. For this particular case, from Eq. (25a) it results $T_1 = \widehat{T}_1$ and the relationships given by Eqs. (27) and (28) are obtained without any approximation.

5. Numerical results

We now illustrate the selfimaging formation properties, discussed in the previous section, by analyzing the RWT of the three following Gaussian periodic pulse trains, all of them having a constant repetition rate $T_1 = 40$ ps, pulse width $T_0 = 2$ ps and a mean wavelength $\lambda = 1550$ nm: (i) $N = 21$ pulses, $C = 0$; (ii) $N = 21$ pulses, $C = -6$; (iii) $N = 129$ pulses, $C = -6$. Accordingly with the analysis done after deriving Eqs. (17) and (18), the pulse train (iii), having a pulse number $|C|$ times greater than (ii), should originate the same selfimage quality as compared with the non-chirped pulse train (i). Following the procedure described in Section 3, we numerically compute the RWT for the three pulse trains and the results are shown in Fig. 2a–c as gray level displays. In order to better visualize the behavior of the pulse trains, a time interval of 100 ps is shown for which only three consecutive central

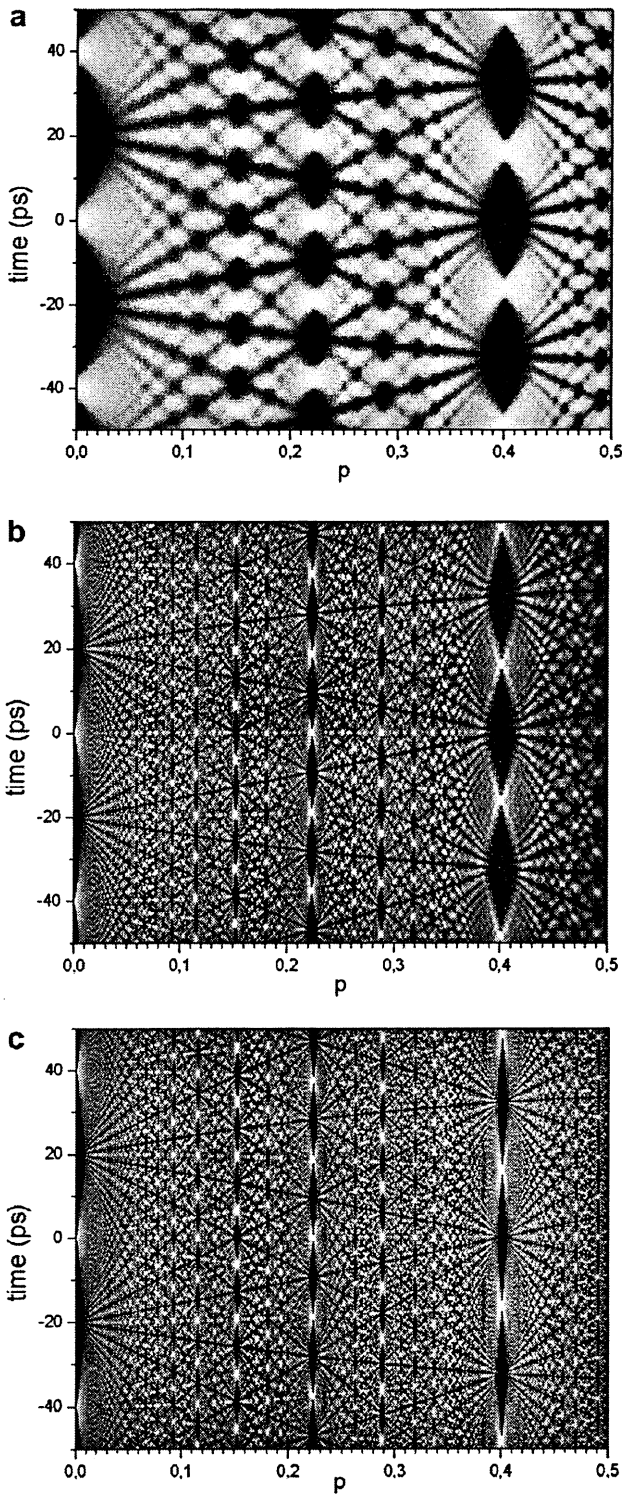

Fig. 2. Gray level displays of the RWT associated with three periodic pulse trains, all of them having a constant repetition rate $T_1 = 40$ ps, a pulse width $T_0 = 2$ ps and a mean wavelength $\lambda = 1550$ nm. In (a) $N = 21$ pulses, $C = 0$; in (b) $N = 21$ pulses, $C = -6$; and in (c) $N = 129$ pulses, $C = -6$. In the three displays, the temporal and fractional order resolutions are $\Delta t = 0.06$ ps and $\Delta p = 0.001$, respectively. For sake of clarity, only three central pulses of the input are shown.

pulses of the input trains can be observed. Besides, for producing well-defined selfimages we restrict the selfimaging orders to be analyzed to the range $0 < p < p_1$, being p_1 the fractional order associated with the first integer selfimage ($s = 1$). For obtaining repetition rate multiplication capability, fractional selfimages are to be also considered for these values of p. For the unchirped pulse train (i), it can be obtained from Eq. (13) $p_1 \approx 0.4004$. By considering this value of p, the RWT displays of Fig. 2 are only shown for $0 < p < 0.5$. Next, we analyze the selfimage irradiances for certain values of the fractional order p. In Fig. 3, the output irradiances $|u_p(t)|^2$ obtained from each RWT display are shown for $p = p_1$. As it is expected, it can be seen in (a) a well-formed selfimage of the pulse train (i) having the repetition period $T_1' = T_1 \times \cos(\pi p_1/2) \approx 32.4$ ps (accordingly with Eq. (12)) and a duty-cycle of 0.05 identical to the input pulse train. In (b), a small distortion in the selfimage of the chirped pulse train (ii) can be observed. Two different distorting effects are present here: the number of pulses should be increased for obtaining a selfimage quality similar to the unchirped case, and the fractional order should be corrected, as it is established by Eq. (27), for chirped pulses. However, as it is shown in (c), the selfimage irradiance of the pulse train (iii), for which the number of pulses is increased by $|C| = 6$, becomes identical to (a) and the mismatch effect in p (due to pulse chirping) is

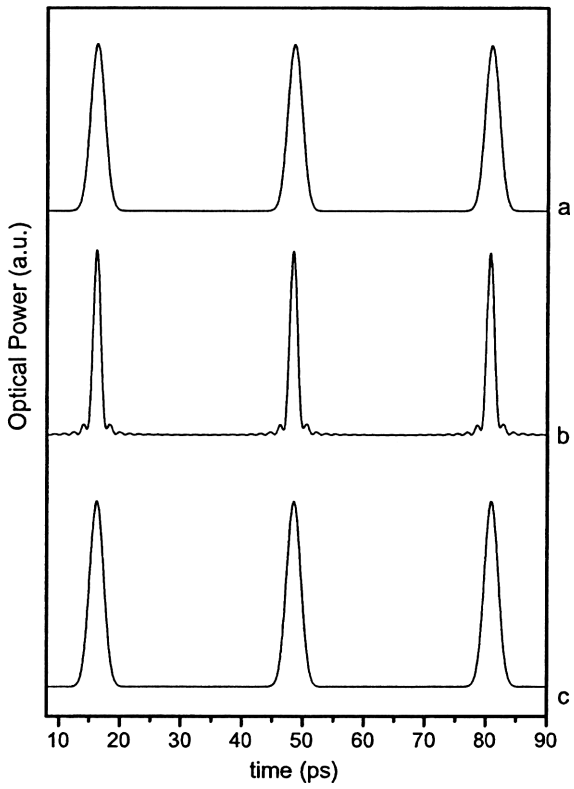

Fig. 3. Output optical powers, associated with the first integer selfimage, obtained from the slices at $p \approx 0.4004$ of each one of the RWT shown in Fig. 2a–c.

negligible. Now, we analyze the irradiances of $|u_p(t)|^2$ for $p \approx 0.0289$. As it can be derived from Eq. (13), this value of p corresponds to the fractional selfimage $s = 1/16$ (i.e., $m = 16$) of the unchirped pulse train (i). The three irradiances are shown in Fig. 4. In (a), the irradiance resembles the input pulse train with a certain distortion level. In this case, the small amount of dispersion Φ_{20} required to obtain $p \approx 0.0289$ is not enough to spectrally overlap the pulses. By inspection of Fig. 2a, it can be concluded that fractional unchirped sefimages can only be observed for $p \geqslant 0.1$. In Fig. 4b and c, the fractional selfimages corresponding to the chirped pulse trains (ii) and (iii) appear severely distorted. In (c), although N is increased by $|C|$ as compared with (b), the mismatch effect in the selection of p (by using Eq. (13) instead of Eq. (27)) becomes relevant. However, as it was discussed after deriving Eqs. (27) and (28), there is an unchirped equivalent pulse train, with repetition period $\widehat{T}_1 = T_1 = 40$ ps and pulse width $\widehat{T}_0 = 2\text{ ps}/\sqrt{1+C^2} \approx 0.33$ ps, which originates the same selfimage irradiances as (ii) and (iii). The RWT of this equivalent pulse train is shown in Fig. 5a, where it can be observed that this display is almost identical to the RWT associated with (iii) (shown in Fig. 2c). To corroborate this equivalence, we derive from Eq. (13) (or equivalently from Eq. (26)) the fractional order for $s = 1/16$ resulting $\hat{p}_S = 0.0289$ (that is the same p as it was used in Fig. 4). By employing Eq. (27), the corrected fractional order associated with $s = 1/16$ for the chirped pulse train results as $p_S \approx 0.0301$. Fig. 5b shows the output irradiance obtained either from the RWT of the chirped pulse train (iii) (shown in Fig. 2c) for $p \approx 0.0301$ or from the RWT of the equivalent unchirped pulse train (shown in Fig. 5a) for $p \approx 0.0289$, so verifying the results found in Section 4. In order to better illustrate the pulse conformation effect, for the chirped and the equivalent unchirped pulse trains, we show in Fig. 6, a small range $0.2218 \leqslant p \leqslant 0.2245$ of the two RWT of Figs. 2c and 5a. This p-range corresponds

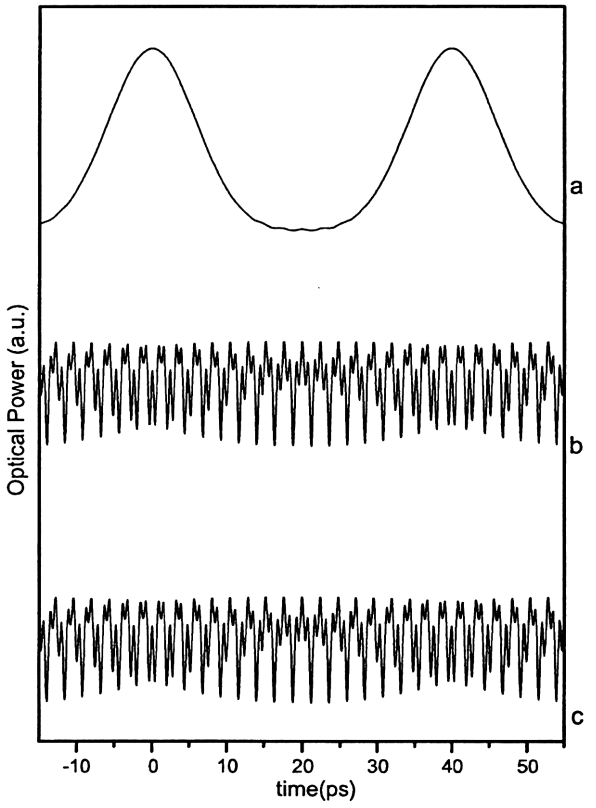

Fig. 4. Output optical powers obtained from the slices at $p \approx 0.0289$ of each one of the RWT shown in Fig. 2a–c. This value of p is associated with the fractional selfimage $m = 16$ of the unchirped pulse train. It can not be observed in (a) (due to the low amount of dispersion Φ_{20} associated with this p), and it is not formed in (b) and (c) due to the shifting effect in the selection of p that should be done for chirped pulses.

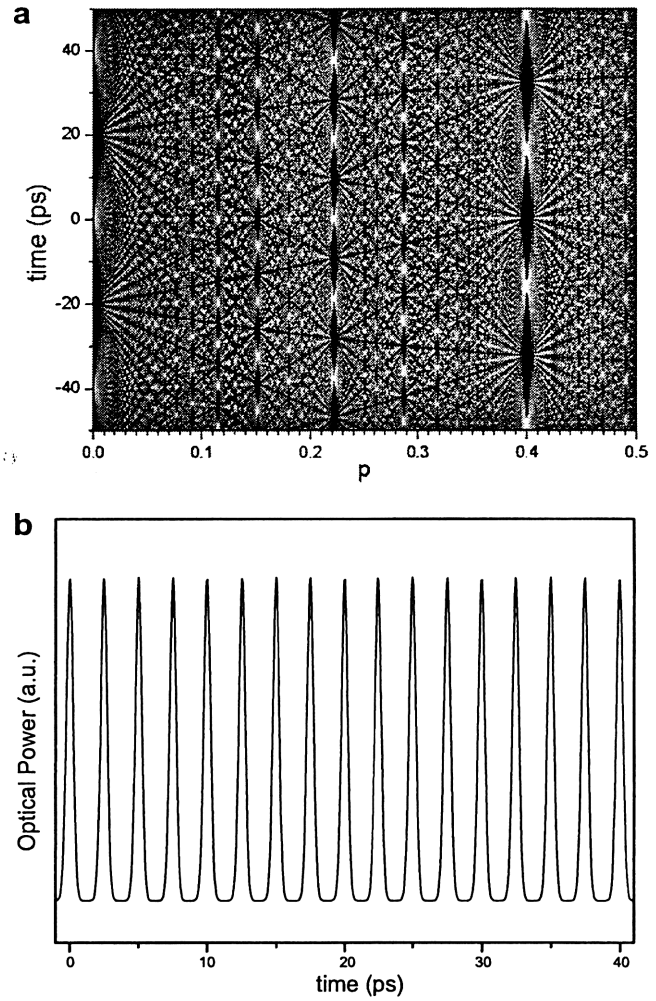

Fig. 5. (a) Gray level display of the RWT corresponding to the equivalent unchirped pulse train (associated with the chirped pulse trains of Fig. 2b and c), having a repetition rate $\widehat{T}_1 = 40$ ps and a pulse width $\widehat{T}_0 \approx 0.33$ ps. The temporal and fractional order resolutions are the same as in Fig. 2 and, for sake of clarity; only three central pulses of the input are shown. (b) Output optical power which can be obtained either from the slice at $\hat{p} \approx 0.0289$ of the RWT shown in (a) or from the slice at the corrected value $p \approx 0.0301$ of the RWT shown in Fig. 2c. Now, a well-defined fractional selfimage $m = 16$ can be observed.

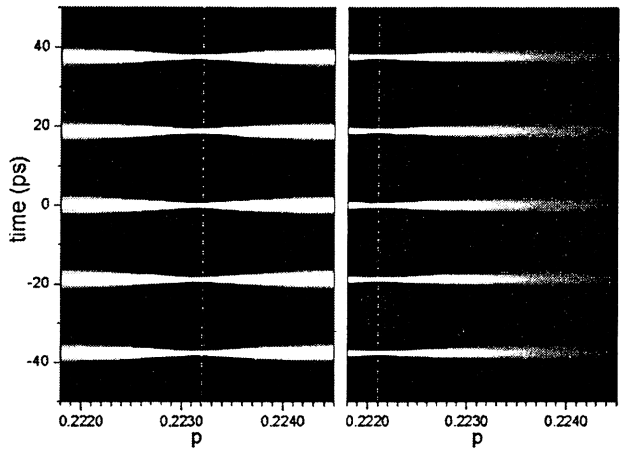

Fig. 6. Enlarged view of the gray level displays of the RWT of Figs. 2c (left side) and 5a (right side). The output optical power corresponding to the fractional selfimage $s = 1/2$ ($m = 2$) can be obtained either from the slice at $\hat{p} \approx 0.2221$ of the RWT (right side) or from the slice at the corrected value $p \approx 0.2231$ of the RWT (left side).

to the fractional selfimage $s = 1/2$ (i.e., $m = 2$). By direct inspection of Figs. 2c and 5a there is no perceptible difference between both RWT displays in the neighborhood of $p \approx 0.22$. However, it can be seen in Fig. 6 that both RWT becomes identical (and so, the associated selfimage irradiances) only for $p_S \approx 0.2232$ (left display, chirped pulses) and $\hat{p}_S \approx 0.2221$ (right display, unchirped equivalent pulses). For other values of p (no satisfying a selfimaging condition), both RWT of Fig. 6 become slightly different. In summary, it can be observed that an additional dispersion is required to observe a selfimage when each optical pulse of the input is chirped, i.e. from $\hat{p}_S \approx 0.2221$ (for $C = 0$) to $p_S \approx 0.2232$ (for $C = -6$). This is so, because when the chirp parameter and the dispersion have opposite signs, the length of the medium can be split in two positive contributions, i.e. $L = L_C + L_T$, assuming that an optic fiber is used as the dispersive medium. The first length of the line (L_C) is used to compress the pulses in the input train individually, and the remaining length of the fiber (L_T) produces the corresponding Talbot selfimage of the compressed pulses train [31].

6. Conclusions

We have presented a method of signal analysis and processing in the time domain based on the RWT description. By employing the space-temporal analogy, a photonic device for producing the temporal RWT was proposed which can be used to originate optical pulses having certain predetermined properties which are of interest in pulse transmission applications in different dispersive media. This approach was applied to analyze several features of the temporal selfimaging or Talbot effect. It was compared the selfimage formation of unchirped and chirped periodic pulse trains. The possibility to obtain, from a certain input periodic train, an output with a higher repetition rate (i.e. selfimages with high fractional order) becomes enhanced by a multiplicative factor ($|C|$), when the input train is chirped. Regarding with the finite extension of the pulse trains, it was found that for obtaining the same selfimage definition, the pulse number of the chirped pulse train should be multiplied by the chirp parameter as compared with the pulse number of the unchirped pulse train. The general relationships linking the pulse train parameters with the fractional orders for which selfimages appear in the RWT were developed for both, unchirped and chirped periodic pulse trains. These results become relevant when fractional selfimages, having high repetition rates, are to be produced since in this case the chirped pulse trains are strongly distorted if they are originated employing the setup parameters associated with the fractional orders corresponding to the similar unchirped condition.

Acknowledgements

This work was supported by Consejo Nacional de Investigaciones Científicas y Técnicas (CONICET - PIP 6156/05), Facultad de Ingeniería, Universidad Nacional de La Plata (UNLP - Project I106), Secretaría de Ciencia y Técnica (SECyT – PICT03-12502) and Comisión de Investigaciones Científicas (CIC 1114/05). CCL and PCC are fellowships of CONICET and CIC, respectively.

References

[1] M.J. Bastiaans, Opt. Commun. 25 (1978) 26.
[2] M.J. Bastiaans, J. Opt. Soc. Am. 69 (1979) 1710.
[3] H.O. Bartelt, K.H. Brenner, A.W. Lohmann, Opt. Commun. 32 (1980) 32.
[4] D. Mendlovic, H.M. Ozaktas, J. Opt. Soc. Am. A 10 (1993) 1875; D. Mendlovic, H.M. Ozaktas, J. Opt. Soc. Am. A 10 (1993) 2522.
[5] A.W. Lohmann, J. Opt. Soc. Am. A 10 (1993) 2181.
[6] L.B. Almeida, IEEE Trans. Signal Process. 42 (1994) 3084.
[7] A.W. Lohmann, B.H. Soffer, J. Opt. Soc. Am. A 11 (1994) 1798.
[8] S. Granieri, O. Trabocchi, E.E. Sicre, Opt. Commun. 119 (1995) 275.
[9] S. Granieri, W.D. Furlan, G. Saavedra, P. Andrés, Appl. Opt. 36 (1997) 8363.
[10] H.M. Ozaktas, Z. Zalevsky, M. Alper Kutay, The Fractional Fourier Transform with Applications in Optics and Signal Processing, Wiley, 2001.
[11] J.C. Woods, D.T. Barry, IEEE Trans. Signal Process. 4 (1992) 3166.
[12] J.C. Woods, D.T. Barry, IEEE Trans. Signal Process. 42 (1994) 2105.
[13] M.J. Bennett, S. McLaughlin, T. Anderson, N. McDicken, IEEE Trans. Biomedical Eng. 53 (2006) 754.
[14] B.H. Kolner, IEEE J. Quantum Electron. 30 (1994) 1951.
[15] A. Papoulis, J. Opt. Soc. Am. A 11 (1994) 3.
[16] C.V. Bennett, B.H. Kolner, IEEE J. Quantum Electron. 36 (2000) 430.
[17] C.V. Bennett, B.H. Kolner, IEEE J. Quantum Electron. 36 (2000) 649.
[18] J. Azaña, L.R. Chen, M.A. Muriel, P.W.E. Smith, Electron. Lett. 35 (1999) 2223.
[19] J. Azaña, M.A. Muriel, Opt. Lett. 24 (1999) 1672.
[20] J. Azaña, M.A. Muriel, IEEE J. Sel. Topics Quantum Electron. 7 (2001) 728.
[21] J. Azaña, L.R. Chen, J. Opt. Soc. Am. B 20 (2003) 1447.
[22] N.K. Berger, B. Levit, A. Bekker, B. Fischer, IEEE Photon. Technol. Lett. 16 (2004) 1855.

[23] J. Lancis, J. Caraquitena, P. Andrés, M.A. Muriel, Opt. Commun. 253 (2005) 156.
[24] C. Cuadrado-Laborde, P.A. Costanzo-Caso, R. Duchowicz, E.E. Sicre, Opt. Commun. 260 (2006) 528.
[25] S. Longhi, M. Marano, P. Laporta, O. Svelto, M. Belmonte, B. Agogliati, L. Arcangeli, V. Pruneri, M.N. Zervas, M. Ibsen, Opt. Lett. 25 (2000) 1481.
[26] J. Azaña, J. Opt. Soc. Am. B 20 (2003) 83.
[27] D.A. Chestnut, C.J.S. de Matos, J.R. Taylor, Opt. Lett. 27 (2002) 1262.
[28] C.J.S. de Matos, J.R. Taylor, Appl. Phys. Lett. 83 (2003) 5356.
[29] J.A. Bogler, P. Hu, J.T. Mok, J.L. Blows, B.J. Eggleton, Opt. Commun. 249 (2005) 431.
[30] C. Cuadrado-Laborde, P.A. Costanzo-Caso, R. Duchowicz, E.E. Sicre, Opt. Commun. 266 (2006) 32.
[31] L. Chantada, C.R. Fernández-Pousa, C. Gómez-Reino, J. Light. Technol. 24 (2006) 2015.